THE JOURNAL OF PHYSICAL CHEMISTRY C

ARTICLE

pubs.acs.org/JPCC

Oxygen Reduction Reaction on Metal-Terminated $MnCr_2O_4$ Nano-octahedron Catalyzing MnS Dissolution in an Austenitic Stainless Steel

Y. J. Wang,[†] P. Hu,[*,‡] and X. L. Ma[*,†]

[†]Shenyang National Laboratory for Materials Science, Institute of Metal Research, Chinese Academy of Sciences, Wenhua Road 72, 110016 Shenyang, China

[‡]School of Chemistry and Chemical Engineering, The Queen's University Belfast, Belfast BT9 5AG, United Kingdom

ABSTRACT: To understand pitting corrosion in stainless steel is very important, and a recent work showed that the MnS dissolution catalyzed by $MnCr_2O_4\{111\}$ is a starting point of pitting. This demonstrates the need to understand the oxygen reduction reaction (ORR) on $MnCr_2O_4\{111\}$, which is the other half-reaction to complete pitting corrosion. In this study, the adsorption behaviors of all oxygen-containing species on $MnCr_2O_4\{111\}$, which has several possible terminations, are explored via density functional theory calculations. It is found that O_2 adsorbs on $MnCr_2O_4\{111\}$ surfaces very strongly. Many possible reactions are investigated and the favored reaction mechanism of ORR is determined. The interactions between O_2 and H_2O on the two metal-terminated $MnCr_2O_4\{111\}$ are found to be different according to the atomic configurations of the two surfaces. All the calculated results suggest that ORR can readily occur on the $MnCr_2O_4\{111\}$ surfaces.

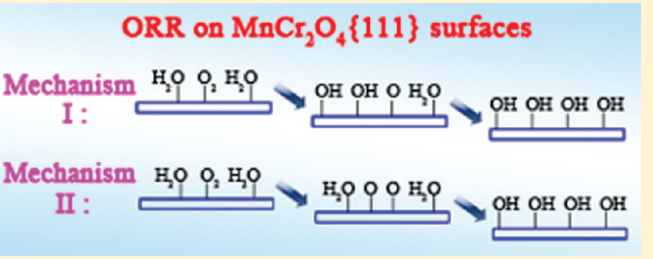

1. INTRODUCTION

It is well-known that the passive film formed on the surface of stainless steel can protect the substrate metal from general corrosion. However, localized corrosions remain serious problems for stainless steel. Among different kinds of localized corrosions, pitting corrosion is the most important because it is considered as the precursor of other localized corrosions.[1] The pitting corrosion process can be divided into two different periods: the nucleation and the growth period. The latter was studied thoroughly experimentally and theoretically because of its relatively larger scale in both temporal and spatial aspects.[2−6] Although there are different opinions regarding the first period, the dissolution of an inevitable inclusion, MnS, was widely accepted as the most possible precursor of pitting corrosion.[7−10] Therefore, to obtain a clear mechanism of MnS dissolution would be necessary for understanding the pitting corrosion of stainless steel. However, knowledge of MnS dissolution remains at the stage of micrometer scale due to the limited spatial resolution of experimental techniques.[11−14]

Recently, we focused on the dissolution of MnS inclusion and designed ingenious transmission electron microscopy (TEM) experiments to record the changes of MnS inclusion before and after the corrosion tests.[15] We found that the dissolution of MnS is indeed localized and the dissolution pits occur on the surface of MnS inclusions, similar in miniature to the corrosion pits of stainless steel. Numerous experiments showed that there are always some nano-octahedrons in the dissolution pits that seem unchanged during the dissolution of MnS, but not all nano-octahedrons could cause pits to form around them.[15]

These nano-octahedrons were identified to be the spinel $MnCr_2O_4$, whose exposed surfaces are all $\{111\}$ surfaces. The result was explained in the framework of contact corrosion, the two electrodes of which are MnS (anode) and $MnCr_2O_4$ (cathode). On the anode, the electrochemical dissolution of MnS occurs, producing Mn^{2+} ions and different S-containing species, such as sulfur, sulfate, and thiosulfate. It is generally accepted that the anodic reaction is catalyzed by the cathode for their special relationship in the corrosion process. The corrosion experiments were executed in neutral NaCl solution, and thus the only possible cathode reaction is the oxygen reduction reaction (ORR). In our last paper,[15] we classified two types of octahedrons with different catalyzing abilities in the thermodynamic aspect. But the detailed kinetics of ORR, such as the barriers of elementary steps, remains unknown. In this paper, ORR information on the active $MnCr_2O_4\{111\}$ surfaces is provided.

ORR is a very important reaction in several areas such as electrochemistry and catalysis. Many efforts have been made to explore its reaction mechanism by ab initio methods.[16−21] The well-accepted mechanisms are the following. In acid media, oxygen

Received: November 12, 2010
Revised: January 14, 2011
Published: February 23, 2011

can be reduced by two- or four-electron reduction reactions:

$$O_2 + 2H^+ + 2e^- \rightarrow H_2O_2 \quad (1)$$

$$O_2 + 4H^+ + 4e^- \rightarrow 2H_2O \quad (2)$$

For the four-electron reduction, two types of mechanisms, dissociative and associative, can be classified if one focuses on the first elemental step. In the dissociative mechanism, the first step is the dissociation of the O−O bond (reaction 3), while the acceptance of a proton and an electron is the first step in the associative mechanism (reaction 4):

$$O_2 \rightarrow 2O \quad (3)$$

$$O_2 + H^+ + e^- \rightarrow OOH \quad (4)$$

In neutral or alkaline media, there are also two- and four-electron reductions

$$O_2 + 2H_2O + 2e^- \rightarrow H_2O_2 + 2OH^- \quad (5)$$

$$O_2 + 2H_2O + 4e^- \rightarrow 4OH^- \quad (6)$$

each with a dissociative or associative mechanism.

To date, most research has focused on ORR on metal surfaces. Considerations of ORR on oxide surfaces are rare. Choi et al.[22] studied ORR on $La_{0.5}Sr_{0.5}MnO_3$ and found that the oxygen adsorption energy is much higher than that on metal surface (2.79 eV on $La_{0.5}Sr_{0.5}MnO_3$ versus 0.72 eV on Pt) and reaction 3 is barrierless. Okamoto[23] investigated ORR on $ZrO_2(\bar{1}11)$ surface and found that spontaneous breaking of the O−O bond in H_2O_2 would occur. To the best of our knowledge, there is no report about ORR on surfaces with the spinel structure in the literature.

$MnCr_2O_4$ is a useful catalyst with a normal spinel structure. It can be used to catalyze the combustion of methane and the decomposition of N_2O and diesel soot.[24,25] Detailed information about the adsorption of oxygen-containing species on $MnCr_2O_4$ surfaces can be very useful to understand the mechanism of these catalysis processes. It is also important for understanding the growth mechanism of various $MnCr_2O_4$ nanostructures.[26]

This paper is organized as follows: Section 2 shows typical results of our experiments. Section 3 describes the methods used in this work. Section 4 gives the adsorption geometries of different oxygen species and describes the processes of ORR. The minimum energy paths of the ORR with discussions about the calculated results are in section 5. Main conclusions are summarized in section 6.

2. EXPERIMENTAL RESULTS ON WHICH THEORETICAL CALCULATIONS ARE BASED

In our recent TEM studies,[15] we identified that fine nano-octahedral precipitates of $MnCr_2O_4$ (with a spinel structure and a space group of $Fd\bar{3}m$) are dispersively distributed in the MnS inclusions. We applied in situ ex-environment transmission electron microscopy and found that MnS initially dissolves at the $MnCr_2O_4$/MnS interface in the presence of salt water. Figure 1 shows a typical example of our experimental results. This figure is taken by use of high-angle annular dark-field (HAADF) technology, which shows the contrasts according to the atom numbers and thickness. In this figure, the brightest area in the lower part is the steel matrix whose atom number is largest,

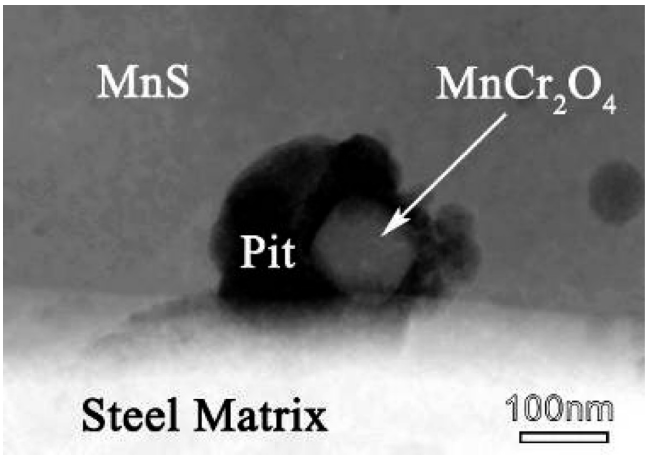

Figure 1. HAADF image showing a pit in MnS around a $MnCr_2O_4$ nano-octahedron.

and the upper area is the MnS inclusion. A black area in the middle of this figure is the dissolution pit in the area of MnS inclusion, and a small particle which is the $MnCr_2O_4$ nano-octahedron can be seen clearly inside the pit.

3. COMPUTATIONAL DETAILS

3.1. Structures of $MnCr_2O_4${111} Surfaces. There are four different atom layers in the direction of ⟨111⟩ if we neglect the trivial fluctuation in the oxygen atom layers. Thus, six different surfaces can be created by cleaving between these layers. The top and side views of these surfaces, named as Cr−O, O−Cr, Mn−O, O−Mn, Mn−Cr′, and Cr′−Mn, are shown in Figure 2. In this study, the Mn−Cr′ and Cr−O surfaces are chosen for the following reasons: (i) According to our previous results, ORR cannot occur on the O−Cr and O−Mn surfaces, noted as O-terminated surfaces.[15] Thus, these two surfaces are excluded. (ii) The other four surfaces are called metal-terminated surfaces and can be classified into two categories, the Cr−O surface and the Mn serial surfaces. In the second category, the Mn−Cr′ surface is chosen because it is a typical metal-terminated surface.

On the Mn−Cr′ surface, there are two types of Mn ions and one type of Cr ions, forming triangle networks. One Mn (Mn1) is on the top site of the subsurface (oxygen atom layer) and the other Mn (Mn2) and the Cr (Cr) are on the hollow sites (Figure 2). Because these triangles consist of different atoms, the three edges of the triangles are obviously not equivalent. They are named as b1, b2, and b3, respectively, marked in Figure 2. In the case of the Cr−O surface, Cr atoms form the 3636 net. There are two types of Cr triangles in this net. In one type of triangles (△1) there is only one oxygen atom under its mass center (hollow site), and in the other one (△2) there are three oxygen atoms under its three edges (bridge sites), shown in Figure 2.

3.2. Construction of Supercells. There are in total six possible oxygen-containing species: O_2, O, H_2O, OH, OOH, and H_2O_2. Two types of surface models were used according to the molecular sizes of oxygen-containing species. The first one is a hexagonal 1 × 1 cell (6.07 Å × 6.07 Å) for O_2, O, H_2O, and OH, the other one is a larger rectangular supercell ($\sqrt{3} \times 1$) for OOH and H_2O_2. The second type of supercell was also used for

dx.doi.org/10.1021/jp1108202 |J. Phys. Chem. C 2011, 115, 4127–4133

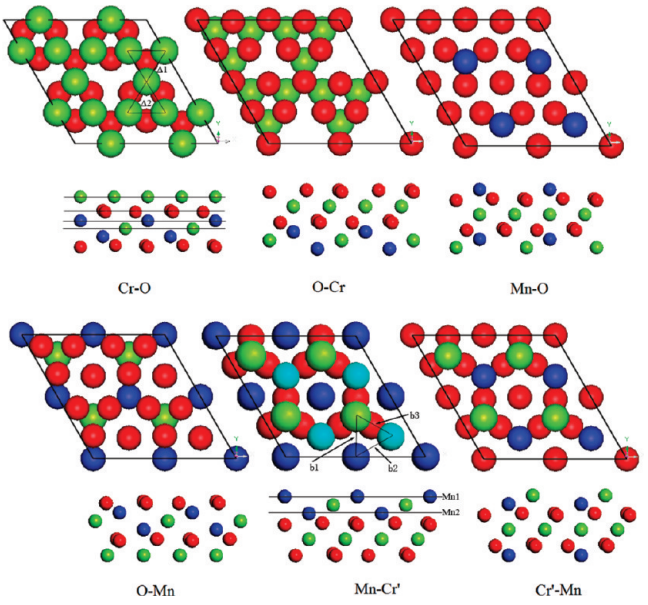

Figure 2. Top and side views of the six different $MnCr_2O_4\{111\}$ surfaces (2×2 supercell). To show the surface structure more clearly, only the top several atom layers are displayed. The six surfaces are named by the element symbols of the top two layers. The first element symbol represents the topmost layer. In the side view of the Cr−O surface, four lines mark the Cr, O, Mn, and Cr′ atom layers from top to down. The blue spheres are Mn atoms and the green and red ones are Cr and O atoms, respectively. In the top view of the Mn−Cr′ surface, Mn2 are colored in light blue to distinguish them from Mn1, and their relative positions in the normal direction are marked in the side view.

the reaction energy and barrier calculations. The surface slab contained 12 layers and half of them were allowed to relax. A vacuum of 12 Å was inserted to separate the periodically repeated slabs. The Monkhorst−Pack **k**-point meshes were $4 \times 4 \times 1$ for the (1×1) cell and $3 \times 4 \times 1$ for the $(\sqrt{3} \times 1)$ cell.

The adsorption energies of different oxygen containing species were calculated according to

$$E_{ads} = E_{slab+adsorbate} - E_{slab} - E_{adsorbate} \quad (7)$$

where $E_{slab+adsorbate}$, E_{slab}, and $E_{adsorbate}$ are the total energies of the surface with an adsorbate, the clean surface, and the adsorbate (O_2 or H_2O) in the vacuum state, respectively. In the cases of O_2, H_2O, and OH radical, the vacuum states can be easily calculated. For the O atom, $E_{adsorbate}$ is taken as $1/2^{Evacuum(O_2)}$. A more negative value of E_{ads} indicates stronger bonding between the surface and the adsorbate.

3.3. Calculations. Spin-polarized calculations were performed by use of Vienna ab initio simulation package (VASP).[27] The Perdew−Wang (PW91)[28] generalized gradient approximation (GGA) functional was utilized with projector-augmented wave (PAW)[29] method. The plane wave cutoff energy was 400 eV. Structures were optimized until the Hellman−Feynman forces on each atom were smaller than 0.05 eV/Å. To reduce the error of polar surfaces, dipole correction was considered. The GGA+U method was used to minimize the error of density functional theory (DFT) calculations for materials containing Cr (U = 3.5) and Mn (U = 4).[30] The bulk $MnCr_2O_4$ was optimized by use of these parameters and the optimized lattice constant is 8.59 Å, which is very close to the experimental value of 8.437 Å. The transition state was searched in the dimer method.[31]

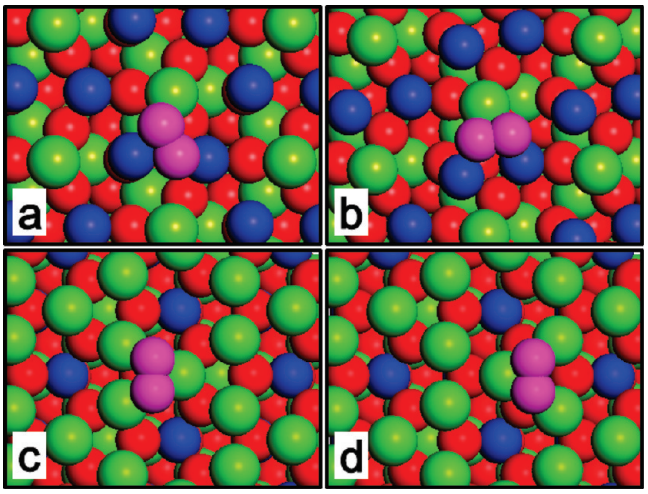

Figure 3. Adsorption geometries of O_2. (a, b) b1-h-b2 and b1-h-b3 structures on the Mn−Cr′ surface. (c, d) Adsorption structures on △1 and △2 of the Cr−O surface. The colors of Mn and Cr atoms are the same as in Figure 2. To distinguish the oxygen atoms in the adsorbed oxygen species and those in the bulk oxide, the former are colored purple. The bond lengths of O_2 in the four geometries are 1.546, 1.504, 1.504, and 1.482 Å, respectively.

Table 1. Adsorption Energies of Four Oxygen-Containing Species on Mn−Cr′ and Cr−O Surfaces

	Mn−Cr′		Cr−O (△1)	Cr−O (△2)
species	sites	energies (eV)	energies (eV)	energies (eV)
O_2	b1-h-b2	−4.114	−4.483	−3.946
O_2	b1-h-b3	−4.017		
H_2O	b1	−0.703	−0.295	−0.400
O	h	−4.003	−2.819	−4.371
OH	b1	−5.188	−4.946	−5.352

4. RESULTS

4.1. Adsorption Geometries of Oxygen-Containing Species. *4.1.1. Molecular Oxygen Adsorption.* The most stable adsorption geometries of O_2 on the Mn−Cr′ and Cr−O surfaces are shown in Figure 3 and Table 1. It was found that, on both surfaces, O_2 adsorbs on the b-h-b sites. On the Mn−Cr′ surface, two types of b-h-b sites are suitable for O_2 adsorption and the adsorption energies of both structures are nearly the same (0.1 eV difference). On the Cr−O surface, there are also two types of b-h-b sites because of the two triangles mentioned above, but the adsorption energies of these two geometries are quite different (0.537 eV difference). The O_2 bond lengths are also reported in Figure 3. Upon comparing them with the DFT-calculated O_2 bond length in vacuum (1.24 Å), it is clear that the O−O bonds are largely stretched on the two surfaces.

4.1.2. O, H_2O, and OH Adsorption. Similar to the case on metal surfaces,[32,33] the most stable adsorption geometries of a single O atom on the Mn−Cr′ and Cr−O surfaces are the hollow sites (Figure 4). On the Mn−Cr′ surface, the O−Mn1, O−Cr, and O−Mn2 bonds are 1.959, 1.957, and 2.209 Å, respectively. On the Cr−O surface, the three O−Cr bonds are 1.930, 2.051, and 2.053 Å on △1 and 1.961, 1.964, and 1.992 Å on △2.

dx.doi.org/10.1021/jp1108202 |J. Phys. Chem. C 2011, 115, 4127–4133

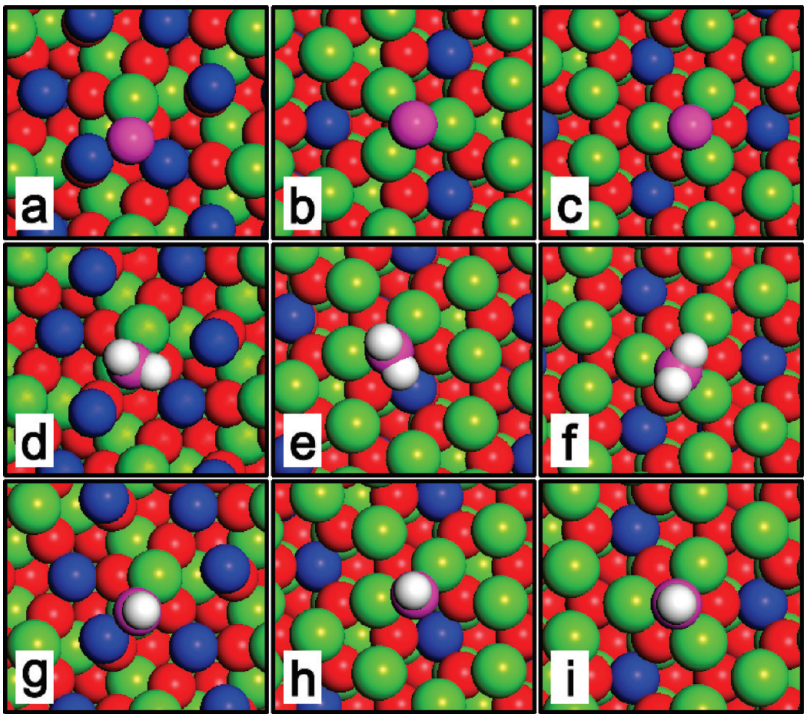

Figure 4. Most stable adsorption geometries of O (a−c), H_2O (d−f), and OH (g−i). The left column (a, d, g) shows adsorption of the three species on the Mn−Cr′ surface. Middle (b, e, h) and right (c, f, i) columns show structures on △1 and △2 of the Cr−O surface. The colors of Mn, Cr, and O atoms are the same as in Figure 3. H atoms are colored white.

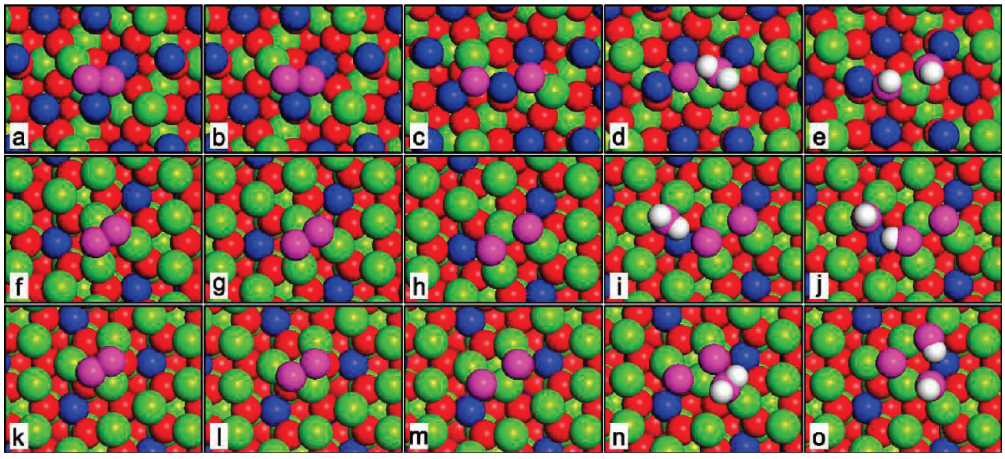

Figure 5. Direct O_2 dissociation and the following protonation on the Mn−Cr′ surface (a−e) and on △1 (f−j), and △2 (k−o) of the Cr−O surface. The first three columns show the initial (a, f, k), transition (b, g, l), and final (c, h, m) states of the direct O_2 dissociation. The fourth and fifth columns show the geometries before and after the relaxation of the protonation process of the first O atom. The protonation of the second O atom is displayed in Figure 6. The color scheme is the same as in Figure 4.

On the Mn−Cr′ surface, H_2O prefers to adsorb on the b1 site, and the molecular plane of H_2O is vertical to the line linking Mn1 and Cr. H_2O is closer to Cr than Mn1, and the O−Cr and O−Mn1 bonds are 2.166 and 2.833 Å, respectively. On the Cr−O surfaces, the most stable adsorption sites of H_2O are the bridge sites on both △1 and △2, and the molecular planes are also vertical to the surface. The only difference is that H_2O on △1 is outside the triangle but H_2O on △2 is inside the triangle.

The adsorption geometries of OH are very similar to those of H_2O on both surfaces. The O−H bonds are always vertical to the surfaces. On the Mn−Cr′ surface, the O−Mn1 bond length is almost the same as the O−Cr bond (2.028 vs 2.059 Å), quite different from the case of H_2O adsorption. On the Cr−O surface, on the other hand, the adsorption site of OH shifts to the hollow site on △2, similar to the case of O adsorption.

4.1.3. OOH and H_2O_2 Adsorption. As they are two possible intermediates in the pathway of ORR, the adsorption geometries of OOH and H_2O_2 were also explored on the two surfaces. It was found that both species were not stable on the two surfaces: their O−O bonds would break during the relaxation. It means that the

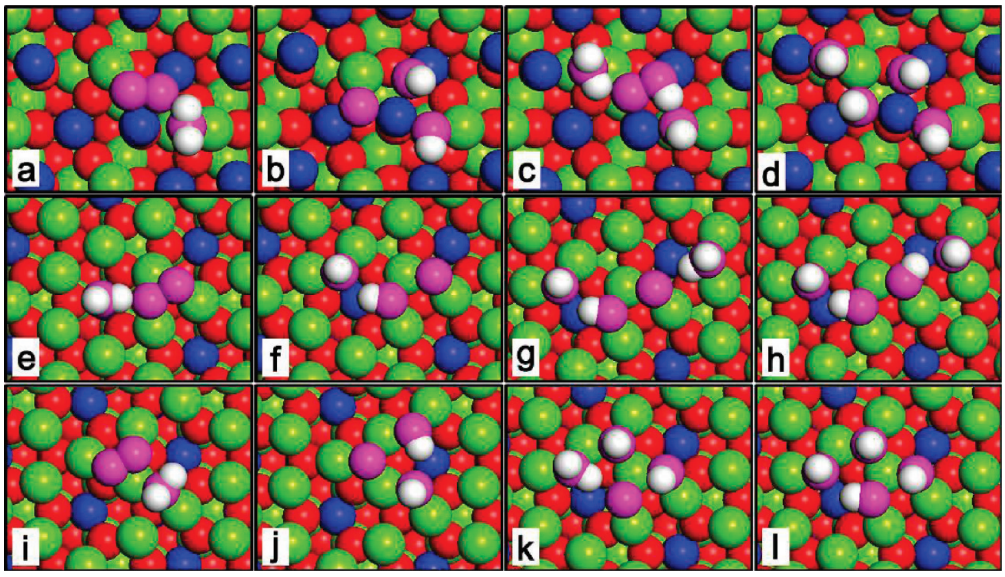

Figure 6. H_2O-assisted O_2 dissociation on the Mn−Cr′ surface (a−d) and on △1 (e−h) and △2 (i−l) of the Cr−O surface. The first column except panel e shows the geometries before relaxation of the first protonation of O_2; panel e shows the transition state of O_2 dissociation in the presence of H_2O. The second column shows the final states of the first protonation of O_2. The third column except panel k shows the geometries before relaxation of the second protonation; panel k shows the transition state of O protonation. The fourth column shows the final states of the second protonation. The color scheme is the same as in Figure 4.

two following reactions can readily occur on the two surfaces:

$$OOH \rightarrow O(ad) + OH(ad) \quad (8)$$

$$H_2O_2 \rightarrow 2OH(ad) \quad (9)$$

4.2. Processes of ORR. *4.2.1. Direct O_2 Dissociation and Protonation.* As mentioned above, O_2 adsorbed on the two surfaces are highly stretched, indicating that the transition state of O_2 dissociation can be reached readily. On the Mn−Cr′ surface, the O−O bond is stretched to 1.695 Å at the transition state and the energy barrier is only 0.024 eV. After the transition state, the two O atoms move away from each other and fall to the hollow sites of the two neighboring triangles (Figure 5). The protonation of the adsorbed O atoms was found to occur readily: When an H_2O is placed on the site shown in Figure 5d, a spontaneous proton transfer process will occur during the relaxation, resulting in two OH adsorbed on b1 of the two triangles.

The O_2 dissociation processes on the Cr−O surface are similar to those on the Mn−Cr′ surface. The barriers of O_2 dissociation on △1 and △2 are 0.070 and 0.137 eV and the corresponding O−O bond lengths are 1.732 and 1.833 Å, respectively. The only major difference is the geometries of the final states. On the Mn−Cr′ surface both O atoms adsorb on the hollow sites, resulting in a stable final state, while on the Cr−O surface the final states are metastable. As mentioned above, the Cr atoms form the 3636 net on the Cr−O surface; namely, the triangles share their edges with the hexagons. Thus, the two O atoms due to the dissociation of O_2 can adsorb only beside the triangles. The distance between the two O atoms on △1 is slightly longer than that on △2 (2.818 vs 2.760 Å).

For the two O adsorbed on △1, if a H_2O molecule is placed on the site shown in Figure 5i, one proton will be transferred to an O atom during the relaxation, resulting in two OH. The protonation of the other O atom is similar, which is shown in Figure 6g,h. On △2, the protonation occurs in a dramatic way: When a H_2O molecule was placed on the site shown in Figure 5n, it would transfer one H atom to one O atom to form two OH. The other O atom moves to the hollow site of △2 and pushes the OH to the bridge site of another △1. The protonation of that O atom needs to overcome a small barrier (0.307 eV).

4.2.2. H_2O-Assisted O_2 Dissociation. It is well-known that the solution environment can affect the kinetics of reactions or even the reaction mechanisms. To further understand the ORR on the surfaces, we studied the solvent effect by adding one H_2O molecule into our system as a rough approximation (the investigation of full solvent effect is beyond the scope of the present work). It was found that the interactions between adsorbed O_2 and H_2O were not the same on the two surfaces.

On the Mn−Cr′ surface, the proton transfer occurs during the relaxation, resulting in one O and two OH adsorbed on the surface. The O atom and one OH sit on their most stable sites, namely, the hollow site and the b1 site, respectively. But the other OH sits on the b2 site. The following protonation of the O atom is the same as that described in section 4.2.1.

On the Cr−O surface, the interaction between O_2 adsorbed on △1 and H_2O is so weak that the protonation occurs only after the O_2 dissociation. This process is also the same as that described in the last subsection (one can compare Figure 5g,j with Figure 6e,f), but the barrier of O_2 dissociation is reduced due to the presence of H_2O (0.004 vs 0.070 eV). After this barrier is overcome, two OH and one O are produced. In the case of △2, O_2 can accept a proton from a nearby H_2O during the relaxation. The transferred proton causes the O_2 to dissociate, producing one O atom on the hollow site of △2 and two OH on the bridge sites of two △1. The following protonation of the O atom on the hollow site needs to overcome a small reaction barrier (0.307 eV). This process is also the same as that described in section 4.2.1.

dx.doi.org/10.1021/jp1108202 |J. Phys. Chem. C 2011, 115, 4127–4133

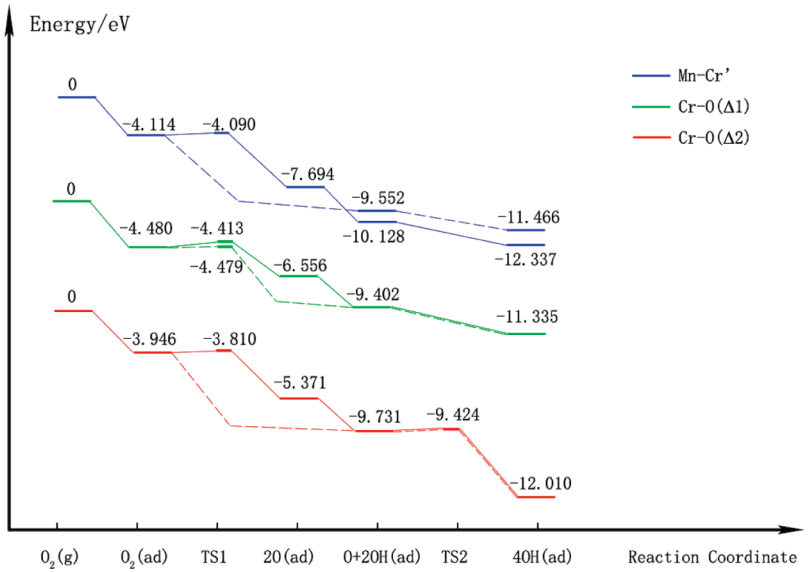

Figure 7. Minimum energy paths (MEPs) of ORR on Mn−Cr′ and Cr−O surfaces. The horizonal bars represent different states and the short ones are transition states. Solid lines show the energy paths through direct dissociation of O_2, and dashed lines show the energy paths through H_2O-assisted O_2 dissociation. The numbers above (or below) the bars are the energy differences between the specific states and the initial states, in electronvolts.

5. DISCUSSION

5.1. Minimum Energy Paths. Figure 7 shows the minimum energy paths of ORR on the two surfaces. TS1 indicates the transition state of O_2 dissociation, and TS2 means the transition state of O protonation. The pure surfaces plus one O_2 and two H_2O molecules in vacuum are considered as the initial states. Take the minimum energy path on the Mn−Cr′ surface as an example. The first state is set as the zero point. The next state is the O_2 adsorption state, with adsorption energy −4.114 eV. After the adsorption, O_2 has two different pathways to dissociate. One pathway is direct dissociation through the transition state (the third bar), resulting in the geometry of 2O adsorbed on the two hollow sites of the surface (the fourth bar). The subsequent protonations of 2O from H_2O molecule produce the O + 2OH adsorbed state (the fifth bar) and the 4OH adsorbed state (the seventh bar). The other pathway is H_2O-assisted dissociation, the products of which are also the O + 2OH and 4OH states. We note that for the O + 2OH and 4OH states, there are different energies for the two pathways. The reason is that, in the second pathway, one OH moves away from its most stable adsorption state, as reported in the last section.

It should be noted that these energies are total energies. To fully describe the processes, one has to calculate the free energies. Two main properties that we did not take into account are the entropies and the zero-point energies, which is a common approach at the moment in the literature. The missing of entropies should mainly introduce errors into the energy differences between initial states and some adsorption states because these energy differences relate to the changing states of molecules between vacuum and adsorption states. The zero-point energies should introduce errors into the energy differences between all states. But considering the energy differences are all very large, these errors may be approximately omitted. The calculated barriers may not be affected largely by the entropies because the geometries of the transition states and corresponding initial states are very similar. The zero-point energy differences between them may also be omitted for the same reason. It should also be mentioned that we described the ORR without a large amount of water. This is, of cause, an approximation as mentioned before. But as a starting point, and as well as a reference, detailed mechanisms reported here are necessary to be known for the following studies, such as the surface phase diagrams in the presence of water and the desorption of OH into the solution. In addition, as discussed below, the main chemistry such as reaction mechanisms obtained from our study should be valid.

5.2. Reaction Mechanisms of ORR. As stated in the Introduction, there are several reaction mechanisms of ORR on metal surfaces, such as two- and four-electron mechanisms, each having an associative or dissociative mechanism, and also acid- or alkaline-media mechanisms. In the system we studied, it is the four-electron mechanism because OH is produced rather than H_2O_2, but whether ORR occurs by the associative or dissociative mechanism depends on the surface structures.

On the Mn−Cr′ surface, the adsorbed O_2 has two ways to complete ORR. One way is direct dissociation with a small barrier, and the other way is to react with a H_2O molecule to form O and 2OH. The second way (reaction 10) occurs during the relaxation and is more favorable than the first way.

$$O_2(ad) + H_2O(ad) \rightarrow O(ad) + 2OH(ad) \qquad (10)$$

Thus, the ORR on the Mn−Cr′ surface is considered to follow the associative mechanism.

On the Cr−O surface, the reaction on △2 is the same as that on the Mn−Cr′ surface. But if O_2 adsorbs on △1 instead, the dissociative mechanism is favored. As reported in the Results section, the interaction between adsorbed O_2 and H_2O is so weak that the direct protonation of O_2 is very difficult. As a result, only if O_2 dissociates to yield atomic oxygen will the protonation occur. The overall reaction mechanism of ORR in our system can be generalized in Scheme 1.

Scheme 1. Reaction Mechanisms of ORR on the Two Surfaces

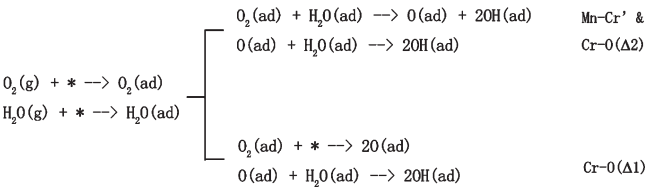

6. CONCLUSION

To fully understand the pitting corrosion of stainless steel, density-functional calculations were performed to investigate the ORR on two types of metal-terminated $MnCr_2O_4\{111\}$ surfaces. The main conclusions are as follows:

(1) O_2 adsorbs on both Mn−Cr′ and Cr−O surfaces strongly. The adsorption geometries in both surfaces are the b-h-b sites.

(2) Barriers for O_2 to dissociate are very low on both surfaces and the further protonation of adsorbed O atoms occurs readily.

(3) Interactions between O_2 and H_2O on the two surfaces are found not to be the same. On the Mn−Cr′ surface and the △2 site of the Cr−O surface, ORR occurs by the associative mechanism. On the △1 site of the Cr−O surface, the protonation can occur only after O_2 dissociation, that is, by the dissociative mechanism.

(4) Calculated barriers and the reactivity of O_2 and H_2O give strong evidence that ORR can occur on the metal-terminated $MnCr_2O_4\{111\}$ surfaces readily.

AUTHOR INFORMATION

Corresponding Author

*To whom correspondence should be addressed. P.H.: Email p.hu@qub.ac.uk. X.L.M.: Email xlma@imr.ac.cn.

ACKNOWLEDGMENT

We thank Professor Y. M. Wang, Dr. S. J. Zheng, Dr. B. Zhang, and Dr. Y.T. Zhou for stimulating discussions. This work was supported by the National Natural Science Foundation of China and National Basic Research Program of China (2009CB623705). P.H. acknowledges the CAS/SAFEA International Partnership Program for Creative Research Teams.

REFERENCES

(1) Laycock, N. J.; Stewart, J.; Newman, R. C. *Corros. Sci.* **1997**, *39*, 1791.
(2) Pickering, H. W.; Frankenthal, R. P. *J. Electrochem. Soc.* **1972**, *119*, 1297.
(3) Laycock, N. J.; Newman, R. C. *Corros. Sci.* **1997**, *39*, 1771.
(4) Budiansky, N. D.; Organ, L.; Hudson, J. L.; Scully, J. R. *J. Electrochem. Soc.* **2005**, *152*, B152.
(5) Scheiner, S.; Hellmich, C. *Corros. Sci.* **2007**, *49*, 319.
(6) Dornhege, M.; Punckt, C.; Hudson, J. L.; Rotermund, H. H. *J. Electrochem. Soc.* **2007**, *154*, C24.
(7) Wranglen, G. *Corros. Sci.* **1969**, *9*, 585.
(8) Eklund, G. S. *J. Electrochem. Soc.* **1974**, *121*, 467.
(9) Stewart, J.; Williams, D. E. *Corros. Sci.* **1992**, *33*, 457.
(10) Baker, M. A.; Castle, J. E. *Corros. Sci.* **1993**, *34*, 667.
(11) Krawiec, H.; Vignal, V.; Oltra, R. *Electrochem. Commun.* **2004**, *6*, 655.
(12) Krawiec, H.; Vignal, V.; Heintz, O.; Oltra, R.; Olive, J. M. *J. Electrochem. Soc.* **2005**, *152*, B213.
(13) Krawiec, H.; Vignal, V.; Heintz, O.; Oltra, R. *Electrochim. Acta* **2006**, *51*, 3235.
(14) Muto, I.; Izumiyama, Y.; Hara, N. *J. Electrochem. Soc.* **2007**, *154*, C439.
(15) Zheng, S. J.; Wang, Y. J.; Zhang, B.; Zhu, Y. L.; Liu, C.; Hu, P.; Ma, X. L. *Acta Mater.* **2010**, *58*, 5070.
(16) Norskov, J. K.; Rossmeisl, J.; Logadottir, A.; Lindqvist, L.; Kitchin, J. R.; Bligaard, T.; Jonsson, H. *J. Phys. Chem. B* **2004**, *108*, 17886.
(17) Wang, Y. X.; Balbuena, P. B. *J. Phys. Chem. B* **2004**, *108*, 4376.
(18) Hyman, M. P.; Medlin, J. W. *J. Phys. Chem. B* **2006**, *110*, 15338.
(19) Vassilev, P.; Koper, M. T. M. *J. Phys. Chem. C* **2007**, *111*, 2607.
(20) Janik, M. J.; Taylor, C. D.; Neurock, M. *J. Electrochem. Soc.* **2009**, *156*, B126.
(21) Ou, L. H.; Yang, F.; Liu, Y. W.; Chen, S. L. *J. Phys. Chem. C* **2009**, *113*, 20657.
(22) Choi, Y.; Lin, M. C.; Liu, M. L. *Angew. Chem., Int. Ed.* **2007**, *46*, 7214.
(23) Okamoto, Y. *Appl. Surf. Sci.* **2008**, *255*, 3434.
(24) Fino, D.; Solaro, S.; Russo, N.; Saracco, G.; Specchia, V. Catalytic removal of methane over thermal-proof nanostructured catalysts for CNG engines. *7th Congress on Catalysis and Automotive Pollution Control*, Brussels, Belgium, 2006.
(25) Fino, D.; Russo, N.; Saracco, G.; Specchia, V. *J. Catal.* **2006**, *242*, 38.
(26) Chen, Y. J.; Liu, Z. W.; Ringer, S. P.; Tong, Z. F.; Cui, X. M.; Chen, Y. *Cryst. Growth Des.* **2007**, *7*, 2279.
(27) Kresse, G.; Furthmuller, J. *Phys. Rev. B* **1996**, *54*, 11169.
(28) Perdew, J. P.; Chevary, J. A.; Vosko, S. H.; Jackson, K. A.; Pederson, M. R.; Singh, D. J.; Fiolhais, C. *Phys. Rev. B* **1992**, *46*, 6671.
(29) Blochl, P. E. *Phys. Rev. B* **1994**, *50*, 17953.
(30) Wang, L.; Maxisch, T.; Ceder, G. *Phys. Rev. B* **2006**, *73*, No. 195107.
(31) Henkelman, G.; Jonsson, H. *J. Chem. Phys.* **1999**, *111*, 7010.
(32) Michaelides, A.; Hu, P. *J. Chem. Phys.* **2001**, *114*, 513.
(33) Michaelides, A.; Hu, P. *J. Am. Chem. Soc.* **2001**, *123*, 4235.